EUROPEAN JOURNAL OF COMPUTATIONAL MECHANICS, 2016
VOL. 25, NOS. 1–2, 71–90
http://dx.doi.org/10.1080/17797179.2016.1181034

Taylor & Francis
Taylor & Francis Group

A NURBS boundary-only approach in elasticity

Vincenzo Mallardo[a] and Eugenio Ruocco[b]

[a]Department of Architecture, University of Ferrara, Ferrara, Italy; [b]Department of Civil Engineering, Design, Building and Environment, Second University of Naples, Aversa, Italy

ABSTRACT

An improvement to the classical application of the isogeometric approach to the two-dimensional boundary element method is proposed. In the classical isogeometric approach the boundary conditions are imposed directly to the control variables that are not always interpolatory of the governing variables, thus introducing an error that may also be large. The issue has been debated in the finite element method context where it has recently motivated various alternative techniques, but it is still open in other numerical methods. In the present paper the approach, introduced by the authors in a previous paper, to correctly impose any general boundary condition in the boundary element method framework, is theoretically and numerically investigated. Comparison with analytical solutions, classical boundary element solutions and isogeometric boundary element solutions are carried out to demonstrate the improved performance of the proposed approach.

ARTICLE HISTORY
Received 25 November 2015
Accepted 13 April 2016

KEYWORDS
Isogeometric analysis; boundary element method; integral equations; boundary conditions

1. Introduction

IsoGeometric Analysis (IGA) has received increasing attention since its first appearance ten years ago (Hughes, Cottrell, & Bazilevs, 2005). The main reason stems from the possibility to take the geometry directly from Computer Aided Design (CAD) programs, avoiding the mesh generation step. Furthermore, the involved functions exhibit high continuity and efficient refinement strategies that allow superior precision and convergence rate.

In the CAD context the geometry is governed by the use of B-Splines and by the Non-Uniform Rational B-Splines (NURBS, see Piegl & Tiller, 1997) curves. From the practical point of view the geometrical representation differs from the classical polynomial shape, commonly adopted in the Computer Aided Engineering (CAE) context, as requiring the definition of control points, knot vectors and weights.

The idea of improving the CAE representation of the domain and of its boundary has been investigated in the last twenty years. Many authors have pointed out the influence of the geometrical representation on the accuracy of the

CONTACT Vincenzo Mallardo mlv@unife.it

solution. For instance in Szabo and Babuska (1991) high-order (*p* version) Finite Element Method (FEM) approaches are demonstrated to show exponential rates of convergence. In this context can be framed the new methodology proposed by Hughes, Cottrell, and Bazilevs (2005) representing the geometry of the domain by NURBS. The procedure is commonly referred as *isogeometric analysis* if the same representation is also adopted to model the governing fields. The FEM methodology has also been extended to the nonlinear analysis. For instance in Verhoosel et al. (2011) isogeometric finite elements are used to introduce the cohesive zone for brittle fracture modelling.

The representation of the boundary of the domain, more than the domain itself, deserves special attention. It holds special interest in some elasticity problems (see for instance Munoz, 2008 in contact analysis). The influence of the boundary's geometrical representation is clearly underlined in Sevilla, Fernández-Méndez, and Huerta (2008) for two-dimensional (2D) analysis and in Sevilla, Fernández-Méndez, and Huerta (2011) for three-dimensional (3D) analysis. In both papers a methodology similar to Hughes, Cottrell, and Bazilevs (2005) is proposed but the NURBS are restricted to the boundary of the computational domain. In such an approach the boundary can be directly imported from any CAD software. Specific interpolation and integration strategies need to be implemented for the elements intersecting the boundary, but a standard finite element approach can be used for the majority remaining part of the domain.

To extend the NURBS approach to the Boundary Element Method (BEM) can be successful. In fact, the governing integral equations involved in the BEM are developed on the boundary only, thus being highly improved by the use of a more accurate representation. The very first application of the isogeometric concept to the BEM is developed in Simpson et al. (2012): The NURBS are adopted to represent boundary, displacements and tractions in 2D elasticity giving rise to what the authors call IGA with the BEM (IGABEM). Related implementation aspects are focused in Simpson et al. (2013). As a matter of fact, all the numerical examples are carried out with reference to geometric shapes and boundary conditions that do not put the issue of the correct imposition of the boundary conditions in evidence. Coupling the isogeometric BEM and T-spline surfaces for linear elastostatic problems is addressed in Peake, Trevelyan, and Coates (2013). An interesting application of the NURBS to the BEM is given in Beer, Marussig, and Duenser (2013) where the isogeometric concept is applied to problems in geotechnical engineering, i.e. exterior problems as typified by analyses of underground excavations. Coupling BEM with the isogeometric concept is worthy to be investigated further as the IGA is able to optimise the main characteristic of BEM, i.e. the capacity to focus the discretisation to the boundary only.

Both in IGABEM and in IGA by FEM the imposition of the boundary conditions needs special attention. If they are homogeneous or inhomogeneous but uniform no problem arises due to the partition of unity property of the NURBS

basis. Non-uniform boundary conditions can be applied to the control points where the NURBS are interpolatory. For all the other cases special treatment has to be employed, similarly to meshless methods. In the FEM context there are a few contributions dealing with this problem. In Wang and Xuan (2010) a transformation method is developed to impose inhomogeneous Dirichlet boundary conditions: the control variables are linked to the collocated nodal values at the essential boundary by previously partitioning the NURBS control points into boundary and interior groups; however this method requires modifications of the stiffness matrix that complicates the usual structure of the FE code. A procedure involving quasi-interpolant projectors is proposed in Costantini et al. (2010) in the context of generalised B-spline-based IGA but no numerical examples are given in elasticity. The Nitsche's method is implemented in Embar, Dolbow, and Harari (2010) for spline-based finite elements. In De Luycker et al. (2011) a weak enforcement of general inhomogeneous Dirichlet boundary conditions using a least squares minimisation is presented.

The present paper intends to propose a novel approach of IGABEM. Any boundary condition, either homogeneous or inhomogeneous, is automatically fulfilled by suitably modifying the final system of equations. Detailed instructions on how it can be implemented in a classical code are given. An analytical/numerical example is provided to show the error introduced by the IGABEM approach in fulfilling the boundary condition, and how such an error does not occur with the present approach. Two more numerical examples are included to demonstrate the capability of the procedure in comparison with the classical BEM and the classical IGABEM. The paper is organised as follows. The next section gives a brief summary of the IGABEM approach. The third section is aimed at presenting the procedure (from now on named ImprIGABEM) with enhanced treatment of the boundary conditions. In the final section, three numerical examples are carried out to demonstrate the efficiency of the procedure.

2. The IGABEM governing relations

In the present section details on the governing integral equations in 2D elasticity and on the IGABEM approach are given. For the sake of clarity a short summary is provided. The discretised integral equations are presented and suitably collocated to generate the final system of equations. Finally the here adopted refinement strategies based on NURBS insertion and knot insertion are detailed.

2.1. Integral equations and NURBS representation

The governing displacement and stress integral equations in linear elasticity have well-known expressions in terms of boundary displacement $\mathbf{u}$, boundary traction $\mathbf{t}$ and Kelvin fundamental solutions $u^*_{ij}(\mathbf{y},\mathbf{x})$, $t^*_{ij}(\mathbf{y},\mathbf{x})$ (see for instance Mallardo & Ruocco, 2014 and Wrobel & Aliabadi, 1996).

In order to solve any general elasticity problem, it is necessary to discretise both the geometry of the boundary and the boundary displacement and traction

fields. Within the IGABEM framework, the same basis functions, i.e. the NURBS, are used for the representation of the geometry and for the approximation of the governing fields.

The definition of the NURBS involves the definition of the B-spline. In fact, the NURBS represent an improvement of the B-splines as they allow, for instance, an exact representation of the conics (such as circle, ellipse, etc.). The NURBS are given by the following relation:

$$R_{i,p}(\zeta) = \frac{w_i N_{i,p}(\zeta)}{\sum_{j=1}^{n} N_{j,p}(\zeta) w_j} \tag{1}$$

where w_j are weights, $N_{i,p}(\zeta)$ is the ith B-spline of degree p (see Piegl & Tiller, 1997 for its expression) and n is the number of control points, i.e. some points (to be discussed further) that fulfil the same task of the mesh nodes in the conventional BEM.

The generation of a B-spline basis of degree p is based on a sequence of real numbers collected in the knot vector:

$$U = (\zeta_1, \cdots, \zeta_{n+p+1}) \tag{2}$$

where $\zeta_1 \leq \zeta_2 \leq \cdots \zeta_{n+p+1}$, and n represents the number of basis functions too. Some of the inner knot spans may have zero length and, often, the knot vector is normalised in $(0, 1)$, i.e. $\zeta_1 = 0$ and $\zeta_{n+p+1} = 1$.

The B-splines are piecewise polynomials and they own some important useful features (see for instance Mallardo & Ruocco, 2014 and Piegl & Tiller, 1997).

The boundary of the elastic domain can be represented by the following expression:

$$\mathbf{x}(\zeta) = \sum_{k=1}^{n} R_{k,p}(\zeta) \mathbf{P}_k \tag{3}$$

where $\mathbf{P}_k$ is the k^{th} control point. First and last control points are coincident if the curve is closed. It is worthy to underline that there is no reason that the control points coincide with boundary points. The main idea of IGABEM is to adopt the same NURBS to describe the governing physical variables, i.e. displacement and tractions on the boundary in the present case:

$$u_l(\zeta) = \sum_{k=1}^{n} R_{k,p}(\zeta) \mathbf{d}_k \tag{4a}$$

$$t_l(\zeta) = \sum_{k=1}^{n} R_{k,p}(\zeta) \mathbf{q}_k \tag{4b}$$

where the vectors $\mathbf{d}_k$ and $\mathbf{q}_k$, of components d_{lk} and q_{lk}, respectively, with $l = 1, 2$ in 2D, will be shortly explained.

The final discretised displacement integral equation, collocated in the node:

$$\overline{\mathbf{y}}_i = \sum_{k=1}^{n} R_{k,p}(\overline{\zeta}_i)\mathbf{P}_k \tag{5}$$

can thus be written as:

$$c_{ij}(\overline{\mathbf{y}}_i)\sum_{k=1}^{p+1} R_{k,p}(\zeta)d_{jk} + \sum_{e=1}^{NE}\sum_{k=1}^{p+1} d_{jk}\left[\int_{\Gamma_e} t^*_{ij}(\overline{\mathbf{y}}_i, \mathbf{x}(\zeta))R_{k,p}(\zeta)J_e(\zeta)d\zeta\right] =$$
$$= \sum_{e=1}^{NE}\sum_{k=1}^{p+1} q_{jk}\left[\int_{\Gamma_e} u^*_{ij}(\overline{\mathbf{y}}_i, \mathbf{x}(\zeta))R_{k,p}(\zeta)J_e(\zeta)d\zeta\right] \tag{6}$$

where the element Γ_e must be intended as the part of curve going from ζ_r to ζ_{r+1} of the knot vector, provided that ζ_r is the e^{th} knot without counting the multiplicity and $\zeta_r \neq \zeta_{r+1}$. NE is the total number of elements and $J_e(\zeta)$ is the Jacobian of the map given by Equation (3) (see also Mallardo & Ruocco, 2014; Simpson et al., 2012 for more details). The collocation nodes can be chosen, for instance, as the Greville abscissae. The unknowns $\mathbf{d}_k$ and $\mathbf{q}_k$ do not represent, as it occurs in conventional BEM, the values of displacement and traction, respectively, in the boundary node, but they are variables that have neither physical meaning nor relation with $\mathbf{u}$ and $\mathbf{t}$. Only one observation can be taken: after $\mathbf{d}$ is computed, the deformed geometry can be drawn by using new control points that are shifted from the initial position of the quantity $\mathbf{d}$.

The final discretised stress relation in any internal point $\mathbf{Y}$ can be written as:

$$\sigma_{ij}(\mathbf{Y}) = \sum_{e=1}^{NE}\sum_{k=1}^{p+1} q_{lk}\left[\int_{\Gamma_e} U^*_{ijl}(\mathbf{Y}, \mathbf{x}(\zeta))R_{k,p}(\zeta)J_e(\zeta)d\zeta\right] -$$
$$\sum_{e=1}^{NE}\sum_{k=1}^{p+1} d_{lk}\left[\int_{\Gamma_e} T^*_{ijl}(\mathbf{Y}, \mathbf{x}(\zeta))R_{k,p}(\zeta)J_e(\zeta)d\zeta\right] \tag{7}$$

Collocating Equation (6) at each collocation point provides the following final system of equations:

$$H\mathbf{d} = G\mathbf{q} \tag{8}$$

where the boundary conditions need to be well-posed in order to compute the unknown displacement and traction on the boundary. The above system of equations can be arranged in order to collect the $2n$ unknowns in $\mathbf{v}_{\Gamma_x}$ (the subscript Γ_x meaning the unknown boundary variables) and the remaining parameters, i.e. the ones associated to the imposed boundary conditions, in $\mathbf{v}_{\Gamma_b}$ (the subscript Γ_b meaning the imposed boundary variables to be collected in the known right-hand side):

$$A\mathbf{v}_{\Gamma_x} = L\mathbf{v}_{\Gamma_b} \tag{9}$$

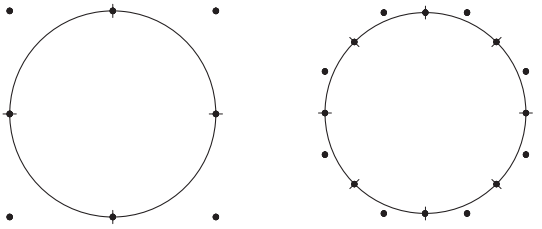

Figure 1. *N*-refinement on the circle. • Control points. - NURBS ends. (a) Four NURBS. (b) Eight NURBS.

Details on the computation of both singular and non-singular integrals can be found in Mallardo and Ruocco (2014).

2.2. N- and h-refinements

In the classical finite-element/boundary-element approach it is rather common to improve the precision of the results either by adding more elements or by increasing the order of the shape functions. The latter is the analogue of the *p*-refinement in the FEM/BEM context. On the other hand, in the isogeometric approach, in addition to the *p*-refinement, the precision can be increased either by dividing the original curve or by inserting new knots. The first strategy is here named *N*-refinement whereas the latter is the analogous of the *h*-refinement in FEM.

The *N*-refinement is obtained by increasing the number of NURBS that reproduce the boundary geometry and the boundary governing displacement and traction fields.

In Figure 1, for instance, the *N*-refinement applied to a circle is depicted. It is worthy to underline that the shape functions do not change, simply the control points are increased (see Figure 2).

The *h*-refinement strategy, at the l^{th} level, inserts l new knots in the original representation without changing the curve geometrically or parametrically. For instance Figure 3 shows the *h*-refinement obtained by inserting one new knot. The new $n+1$ basis functions and new $n+1$ control points are formed recursively from the previous representation of n basis functions and n control points (see Hughes, Cottrell, & Bazilevs, 2005 for details).

The curve after *h*-refinement is geometrically and parametrically identical to the original curve but the basis functions and the control points are changed (see Figure 4).

The different representation between *N*- and *h*-refinement is more evident if a stress concentration occurs. The convergence to the maximum (analytical) vertical stress arising in an infinite plate with an elliptical hole (Figure 5) can be tested by both refinement strategies with different ratios $\frac{a}{b}$. It is worthy to remind that for such a geometry a very poor discretisation is sufficient to model exactly

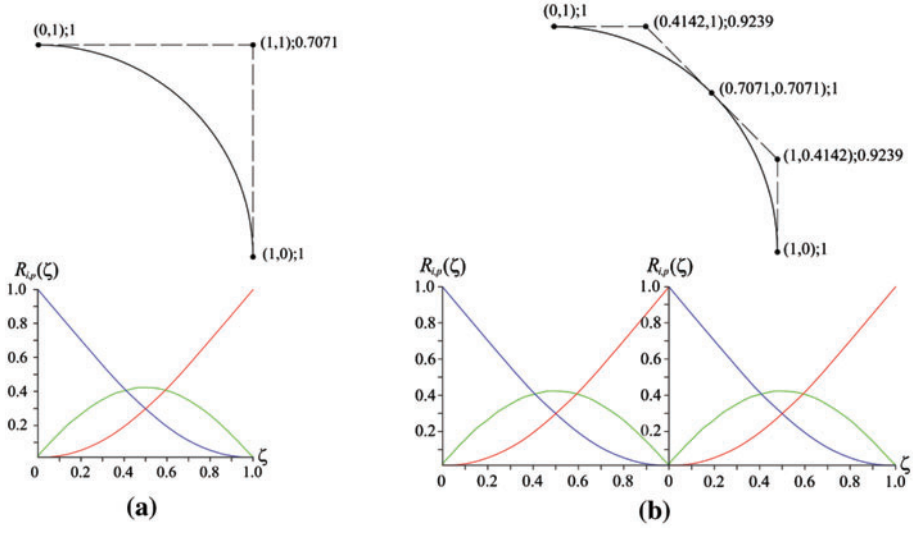

Figure 2. A quarter-circle represented by one NURBS (a) and by two NURBS (b): geometry (above) and the corresponding quadratic NURBS (below).

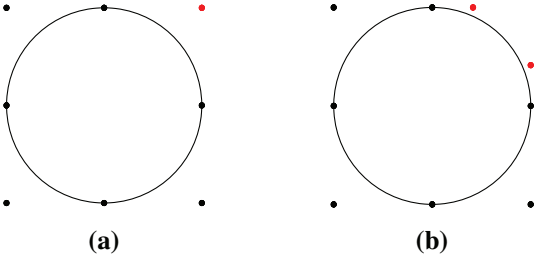

Figure 3. From (a) to (b): *h*-refinement on the circle with insertion of one knot. • Control points. • • Control points involved by the knot insertion.

the geometry and, therefore, the occurring numerical error is mainly related to the field variables representation (displacement and traction).

The numerical finite domain is obtained by considering a limited plate of size 80 times larger than the major ellipse axis (see Figure 5). The following mechanical and geometrical parameters and load condition are adopted: Young's modulus $E = 10^5$, Poisson's coefficient $\nu = 0.3$, $a = 1$ and $p = 1$. In Figure 6, the convergence of the N- and h refinements is tested with respect to the maximum analytical stress given by:

$$\sigma_{max} = p\left(1 + 2\frac{a}{b}\right) \tag{10}$$

for different values of a and b of the ellipse and versus the Degree of Freedom (DoF) of the numerical model. The higher a/b is, the stronger is the effect of the stress concentration as the ellipse tends to the penny shaped crack.

The filled symbol in the figure refers to the results obtained by the h-refinement, whereas the empty symbol refers to the N-refinement. The error of a few percent

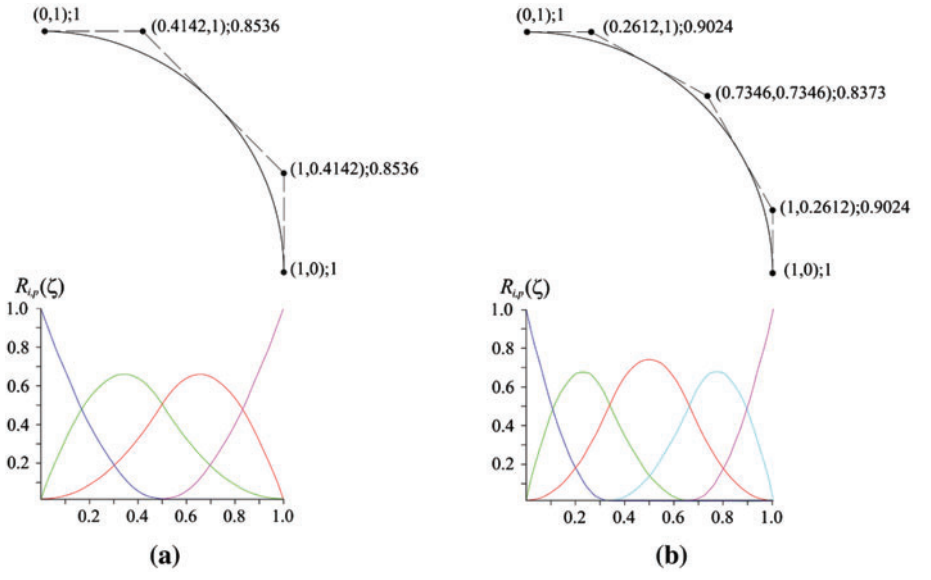

Figure 4. *h*-refinement with one knot insertion: geometry (above) and the corresponding quadratic NURBS (below). (a) Four knots. (b) Five knots.

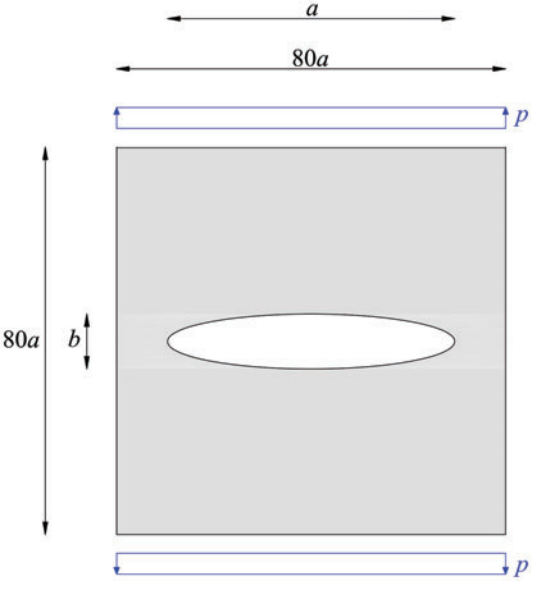

Figure 5. Elliptical hole within an infinite plate under traction.

for very fine meshes (over 200 DoF) is mainly due to the fact that the numerical domain has been limited to 80 times the elliptical hole and it is not of infinite size. The results demonstrate that the *h*-refinement provides more reliable stress results.

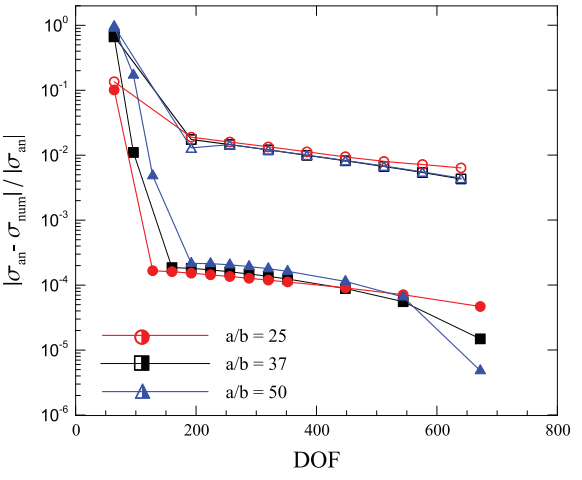

Figure 6. Stress error norm for plate with elliptical hole. Comparison between *N*- (empty symbol) and *h*- (filled symbol) refinement strategies.

3. Boundary condition enforcement

To apply inhomogeneous boundary conditions at the spatial locations of non-interpolatory control points introduces an error that reduces the overall accuracy. In the present section a new procedure is provided to overcome such a issue. The main relations are here reported. Furthermore, some implementation aspects are discussed to show that the procedure can be easily implemented in a classical IGABEM code.

Let us consider general mixed boundary conditions that can be imposed to each collocation point. The $2n$ imposed scalar values, either traction component or displacement component, can be collected in a vector $\overline{\mathbf{w}}$ that can be expressed as:

$$\overline{\mathbf{w}} = B\mathbf{v} \tag{11}$$

where $\mathbf{v}$ is a vector collecting all the variables $\mathbf{d}$ and $\mathbf{q}$ and B is a ($2n$ x $4n$) matrix whose half entries only need to be computed because some of them are zero. For instance, in the special case of Dirichlet (Neumann) conditions, the left (right) part of B is zero. The matrix B can be rearranged in order to collect the final unknowns and the parameters involved by the boundary conditions in two sub-vectors $\mathbf{v}_{\Gamma_x}$ and $\mathbf{v}_{\Gamma_b}$ (already defined in Equation (9)), respectively:

$$\overline{\mathbf{w}} = \begin{bmatrix} B_{\Gamma_x} & B_{\Gamma_b} \end{bmatrix} \begin{pmatrix} \mathbf{v}_{\Gamma_x} \\ \mathbf{v}_{\Gamma_b} \end{pmatrix} \tag{12}$$

By applying a suitable matrix condensation to Equation (9), the final squared system of equations, with the correct imposition of the boundary conditions, can

be obtained:

$$\mathbf{v}_{\Gamma_b} = -B_{\Gamma_b}^{-1} B_{\Gamma_x} \mathbf{v}_{\Gamma_x} + B_{\Gamma_b}^{-1} \overline{\mathbf{w}} = C\mathbf{v}_{\Gamma_x} + \mathbf{a} \Longrightarrow (A - L\,C)\mathbf{v}_{\Gamma_x} = L\mathbf{a} \Longrightarrow \overline{A}\mathbf{v}_{\Gamma_x} = \mathbf{b} \tag{13}$$

From the computational point of view, the above procedure can be implemented in a more efficient way. Displacement and traction in the collocation nodes belonging to the generic NURBS of the discretised boundary can be written in matrix form in terms of the N variables $\mathbf{d}_k$ and $\mathbf{q}_k$:

$$\mathbf{u} = C\mathbf{d} \tag{14a}$$

$$\mathbf{t} = C\mathbf{q} \tag{14b}$$

where $\mathbf{u} = (\mathbf{u}(\overline{\mathbf{y}}_1), \cdots, \mathbf{u}(\overline{\mathbf{y}}_N))^T$ and $\mathbf{t} = (\mathbf{t}(\overline{\mathbf{y}}_1), \cdots, \mathbf{t}(\overline{\mathbf{y}}_N))^T$, ($T$ meaning transpose), and the matrix C is given by:

$$C = \begin{pmatrix} C_{11} & \cdots & C_{1N} \\ \vdots & \vdots & \vdots \\ C_{N1} & \cdots & C_{NN} \end{pmatrix} \tag{15}$$

whose 2×2 submatrix C_{ik} contains one scalar term that can be easily computed:

$$C_{ik} = \begin{pmatrix} R_{k,p}(\overline{\mathbf{y}}_i) & 0 \\ 0 & R_{k,p}(\overline{\mathbf{y}}_i) \end{pmatrix} \tag{16}$$

The Equation (14) can be inverted:

$$\mathbf{d} = C^{-1}\mathbf{u} \tag{17a}$$

$$\mathbf{q} = C^{-1}\mathbf{t} \tag{17b}$$

On the basis of the above steps, the system of Equation (8) can be written in terms of displacement and traction on the boundary:

$$\tilde{H}\mathbf{u} = \tilde{G}\mathbf{t} \tag{18}$$

In fact, the global matrices $\tilde{H}$ and $\tilde{G}$ are built by suitably inserting the $2N \times 2N$ submatrices $\tilde{H}_{\text{NURB}}$ and $\tilde{G}_{\text{NURB}}$, respectively, for all the NURBS describing the boundary of the problem under analysis. Each couple of submatrices $\tilde{H}_{\text{NURB}}$, $\tilde{G}_{\text{NURB}}$ is easily computed by:

$$\tilde{H}_{\text{NURB}} = H_{\text{NURB}} C^{-1} \tag{19a}$$

$$\tilde{G}_{\text{NURB}} = G_{\text{NURB}} C^{-1} \tag{19b}$$

In the special case that a constant traction component is applied on Γ_{NURB} (i.e. one NURBS of the boundary Γ):

$$t_l(\overline{\mathbf{y}}) = K \text{ with } K = \text{ constant value } \forall\, \overline{\mathbf{y}} \in \Gamma_{\text{NURB}} \tag{20}$$

then Equation (17b) implies:

$$q_l(\overline{\mathbf{y}}) = K \,\forall\, \overline{\mathbf{y}} \in \Gamma_{\text{NURB}} \tag{21}$$

due to the partition unity property of the NURBS. In all the other situations, an error occurs when the boundary condition is applied directly to q_l rather than to t_l.

It is worthy to remark some issues.

Remark 1. The inversion of the matrix C is not numerically carried out, as it is achieved by solving the system of Equation (14) with given boundary conditions.

Remark 2. The resolution of the system (14) is performed for each NURBS and not for the entire boundary, i.e. the dimension of the matrix C is limited.

Remark 3. C is positive and banded (with bandwidth equal to $p + 1$) with consequent benefit from reduced storage and faster resolution algorithms, both in 2D and in 3D.

4. Numerical results

In the present section three numerical examples are investigated to demonstrate both the reliability and the efficiency of the proposed procedure (ImprIGABEM) and its superior performance when compared to the current procedure (IGABEM). The reported error norms in terms of displacement are computed in L_2 sense and normalised with respect to their corresponding norms obtained from the analytical solution, i.e.

$$e = \frac{\|\mathbf{u} - \mathbf{u}_{an}\|_{L_2}}{\|\mathbf{u}_{an}\|_{L_2}} \tag{22}$$

The first example (see Figure 7) deals with a benchmark cantilever problem in plane strain for which an analytical solution is available. It is aimed at investigating the error arising in the numerical boundary conditions when using the classical approach and how such an error is avoided with the present approach.

Other two numerical examples are aimed at comparing ImprIGABEM and IGABEM for general curved boundaries (note that the example in Section 3 has straight boundaries). In order to do so, two infinite-size 2D structural problems for which an analytical solution is provided are investigated. The availability of the analytical solution allows a complete comparison. The former example (see Figure 10) deals with a hole in an infinite plate subjected to unidirectional tension at infinity, the latter (see Figure 15) solves the semi-infinite L-shaped wedge in mode I loading case. These geometries are usually converted into finite-size

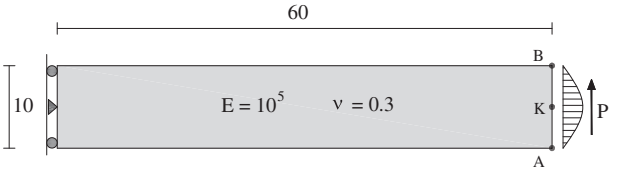

Figure 7. Cantilever beam under parabolic shear load at one end.

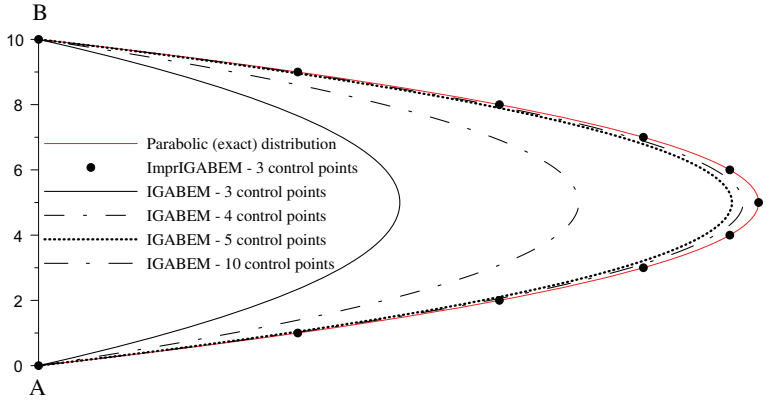

Figure 8. Computed applied traction on the AB side of the cantilever beam. Comparison between IGABEM, ImprIGABEM and exact value.

problems by invoking the symmetry (dash-point line in Figure 9), trimming the infinite plate along straight lines (Γ in the Figure 9) and applying the exact traction on the trimming lines. The numerical domain is eventually the dark-grey domain in Figure 9.

The approach described in the present paper reveals its superiority when either the boundary of the structure under analysis is loaded by non-homogeneous Dirichlet/Neumann conditions or the more the boundary geometry is curved. These two conditions can occur in a huge amount of structural problems but, to the authors' opinion, they can be focused by solving the two infinite-size examples introduced above in the following way: the trimming line Γ is drawn with increasing curvature and the numerical results compared for different curvature level. Such a convergence study can well highlight the difference in precision between the proposed approach (ImprIGABEM) and the usual approach (IGABEM) for general curved boundary, with the additional advantage to have the analytical solution available.

4.1. Cantilever beam

The plane strain benchmark cantilever beam depicted in Figure 7 is considered. The geometry and the material properties are listed in the figure. The corresponding analytical y-displacement of the point K (middle point of AB, see

Table 1. Comparison of P between the present approach (ImprIGABEM) and the classical (IGABEM) approach (c.p. stands for *control points* on *AB*). P= 1 is the correct value.

	ImprIGABEM	IGABEM			
	3 c.p.	3 c.p.	4 c.p.	5 c.p.	10 c.p.
P	1.0	0.5	0.750	0.870	0.979

Figure 7) is:

$$u_y(K) = \frac{P}{6\overline{E}I}\left[2L^3 + (4+5\overline{\nu})\frac{H^2L}{4}\right] \tag{23}$$

where $I = H^3/12$ and:

$$\overline{E} = \frac{E}{1-\nu^2}\,\overline{\nu} = \frac{\nu}{1-\nu} \tag{24}$$

The Equation 4(b) provides the actual boundary traction on AB in terms of the variables $\mathbf{q}$ associated to the control points. In the classical approach, the boundary condition on the side AB of the cantilever would be imposed on q_y. The correct value of the traction in K is $\frac{3P}{2H}$, whereas if, for instance, one element is adopted along AB, the value obtained by imposing the boundary condition on q_y would be:

$$t_y(K) = R_{2,2}(K)q_y(K) = 0.5q_y(K) = 0.5\frac{3P}{2H} = \frac{1}{2}t_{y_{correct}}(K) \tag{25}$$

exactly one half of the correct value. The inconvenience is commonly overcome by increasing the number of elements. On the contrary, the approach proposed by the present paper is correct without any need to increase the mesh. The integral of the boundary conditions on the loaded side of the cantilever beam versus increasing number of control points is a measure of the error introduced by the uncorrect imposition of the boundary conditions. From Table 1 it is evident that three control points on AB are sufficient in the proposed approach (ImprIGABEM) to obtain exactly $P = 1$ whereas 10 control points are necessary to provide about 98% of P with the classical IGABEM. The integration is carried out by Gaussian quadrature with twelve points. Eight elements on the horizontal sides of the beam and four elements on the fixed vertical side of the beam are used. The error in the computation of P is also highlighted in Figure 8 where the y-component of the applied traction on AB modelled by the present approach (ImprIGABEM) and by the classical IGABEM approach are compared with the correct value. The superior performance of the present approach is evident.

The error introduced by the classical IGABEM and overcome by the present approach is reflected into the displacement solution. In Table 2 the analytical displacement of the point K is compared to the value obtained with three control points by the present approach and to the values computed by the classical IGABEM approach with increasing number of control points (i.e. applying h-refinement). In conclusion the way by which the classical IGABEM approach

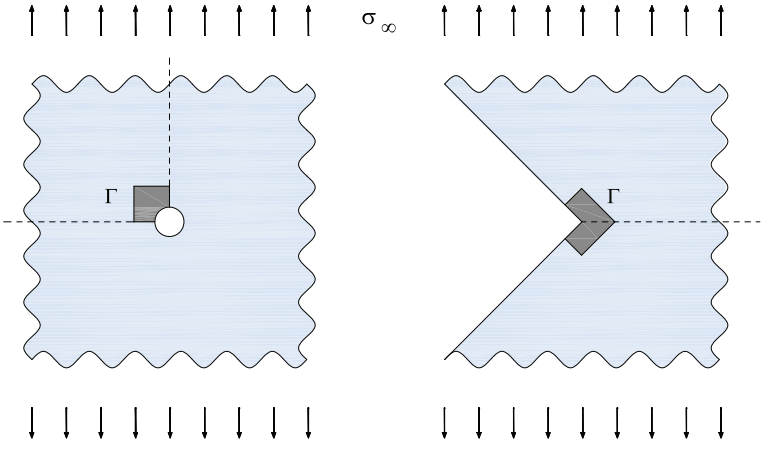

Figure 9. Usual extraction of the numerical finite domain from the infinite domain of the analytical solution. Hole in an infinite plate (left). Semi-infinite L-shaped wedge (right).

Table 2. Comparison of $u_y(K)$ between the present approach (ImprIGABEM) and the classical IGABEM approach (c.p. stands for *control points* on *AB*).

		ImprIGABEM	IGABEM			
	Analytical	3 c.p.	3 c.p.	4 c.p.	5 c.p.	10 c.p.
$u_y(K) * 10^{-3}$	8.03	8.06	4.03	6.03	6.99	7.86

imposes the non-homogeneous boundary conditions introduces an error that can be overcome only by deeply refining the mesh. The approach proposed by the present paper is able to provide a numerical solution that is clear of such an error.

4.2. Hole within an infinite plane

The problem of an infinite plate with a hole under the action of a unidirectional tension σ_∞ has an analytical solution that is available, for instance, in Szabo and Babuska (1991). Plane strain condition is adopted. The mechanical parameters are: Young's modulus $E = 10^6$ and Poisson's coefficient $\nu = 0.3$. The prescribed boundary conditions at infinity are $\sigma_\infty = 1.0$ and the size of the internal hole's radius is $R = 1.0$.

The boundary conditions on Γ (see Figure 9-left) are computed as exact tractions $\mathbf{t}_\Gamma$:

$$\mathbf{t}_\Gamma = T_{an}\mathbf{n} \tag{26}$$

whereas zero-displacement conditions are applied at the symmetry lines. The analytic stress tensor T_{an} can be found in Szabo and Babuska (1991) (see Eqs. 10.40). The numerical results concerning two different shapes of the curve Γ are presented here. The curve Γ is compound by (red line in Figure 10) either two straight lines or a quarter-circle.

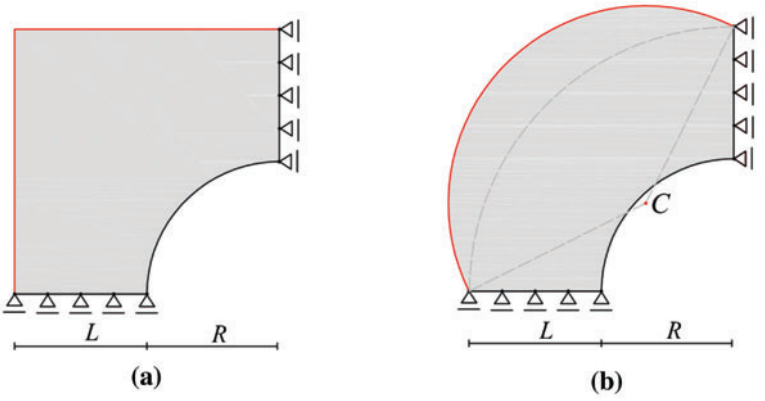

Figure 10. Two different finite domains extracted by the infinite plate with hole: (a) two straight lines, (b) quarter-circle.

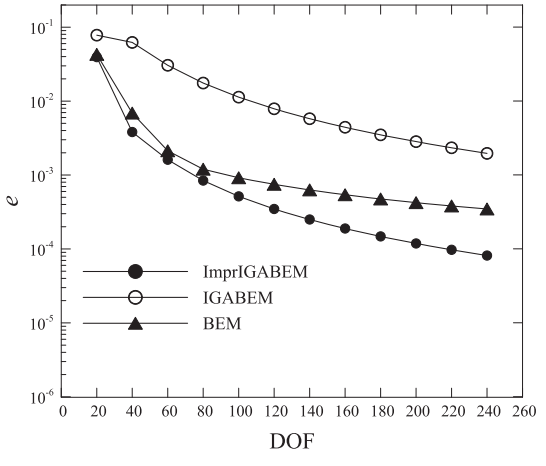

Figure 11. Error *e* plot for infinite plate with hole. Boundary straight lines.

First of all a comparison can be made between the present ImprIGABEM approach, the classical BEM and the classical IGABEM, in terms of the convergence performance in the case of Γ = straight line. If L is the size depicted in Figure 10(a), Figure 11 compares the convergence rate for $L = 2$ in terms of the total number of DoF reported along the x-axis.

From Figure 11 it is worthy to observe that a lower error is obtained with the present approach.

The comparison can be also carried out by replacing one boundary line with a circle arc (see Figure 10(b)) and L from 2 to 200. The corresponding convergence diagrams are depicted in Figure 12.

In such a case the error introduced by an uncorrect imposition of the boundary condition is more evident and it does not become negligible as L increases because the boundary conditions do not analytically tend to the constant value. The error

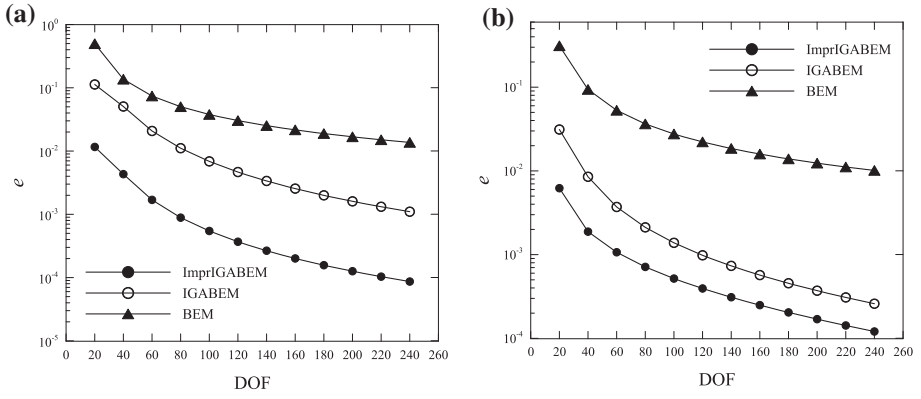

Figure 12. Error e plot for infinite plate with hole. Quarter-circle boundary. (a) $L = 2$, (b) $L = 200$.

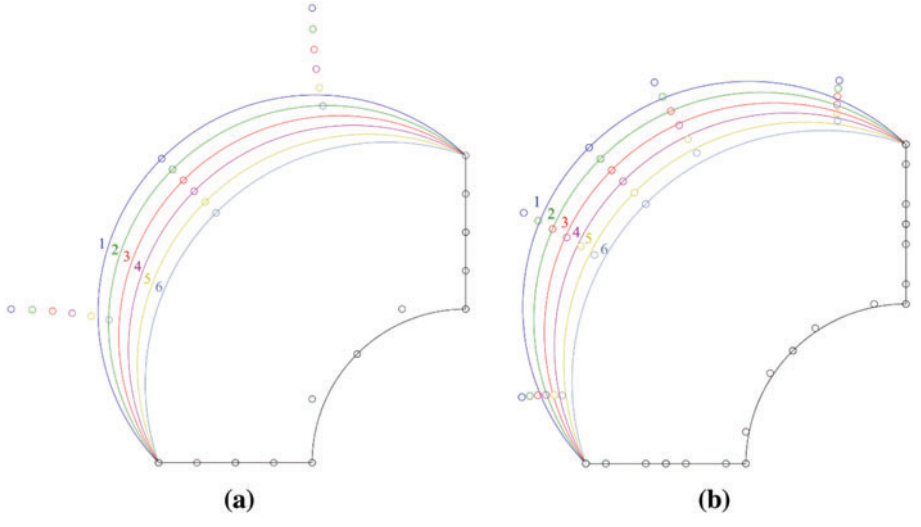

Figure 13. Quarter-circle boundary Γ with different curvatures. The circles indicate the control points. (a) 32 DoF, (b) 48 DoF.

introduced by an uncorrect imposition of the boundary conditions increases with increasing curvature. With reference to the six different arcs depicted in Figure 13, the comparison in error e is shown in Figure 14 with 32 elements in (a) and 48 elements in (b).

From such results it is clear that the difference between the proposed ImprI-GABEM approach and the classical IGABEM approach increases as the control points distance from the boundary (i.e. arc-type going from 6 to 1).

4.3. Semi-infinite L-shaped wedge

The present problem deals with the semi-infinite L-shaped wedge (see Figure 15) which exhibits a singularity at the wedge apex. The analytical solution is available

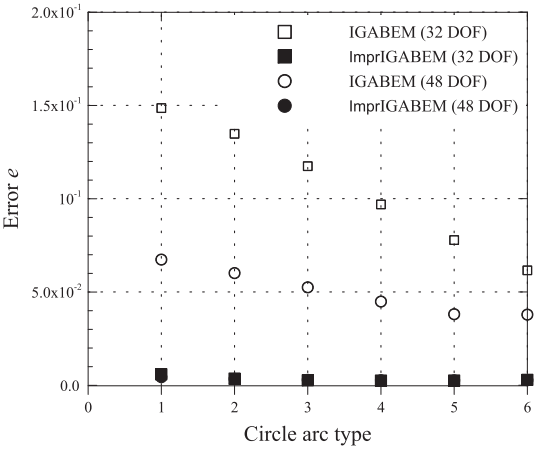

Figure 14. Error e plot for different circular arcs Γ (see Figure 13).

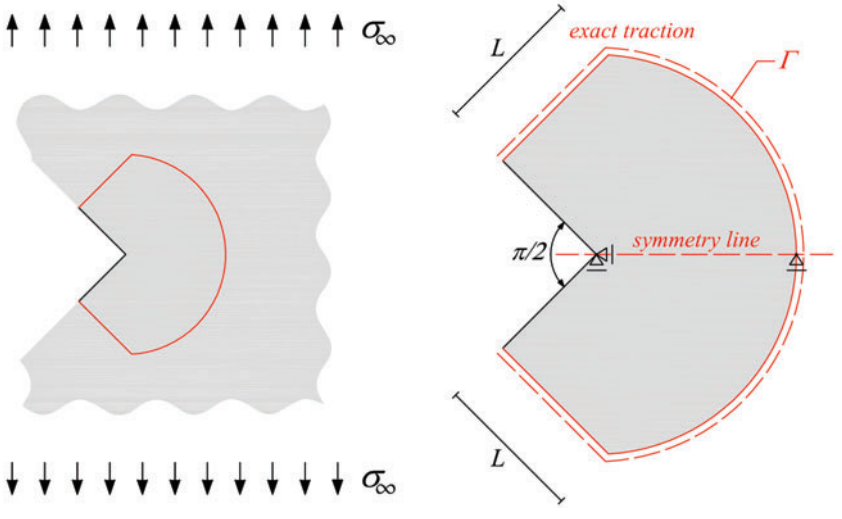

Figure 15. Semi-infinite $\pi/2$ wedge under uniform traction.

in Szabo and Babuska (1991) (see Eqs. 10.27). Mode I loading case in plane strain with the following parameters $L = 1$, $E = 10^5$, $\nu = 0.3$, $\sigma_\infty = 1$, is considered.

The problem is numerically solved by cutting the boundary along the boundary Γ as depicted in Figure 15. The analytical tractions can be applied along these lines as boundary conditions of the numerical problem. In Figure 16 the results corresponding to the classical BEM, to the classical IGABEM and to the proposed ImprIGABEM are compared. Better results are obtained with the proposed procedure.

In Figure 17 the error:

$$\frac{|\,\mathbf{u} - \mathbf{u}_{\text{an}}\,|}{|\,\mathbf{u}_{\text{an}}^{\max}\,|} \tag{27}$$

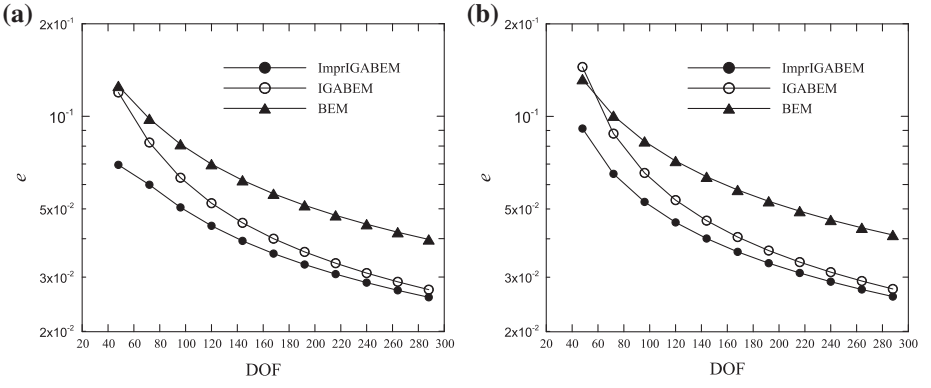

Figure 16. Error e plot for semi-infinite L-shaped wedge. Circular boundary line. (a) $L = 1$, (b) $L = 100$.

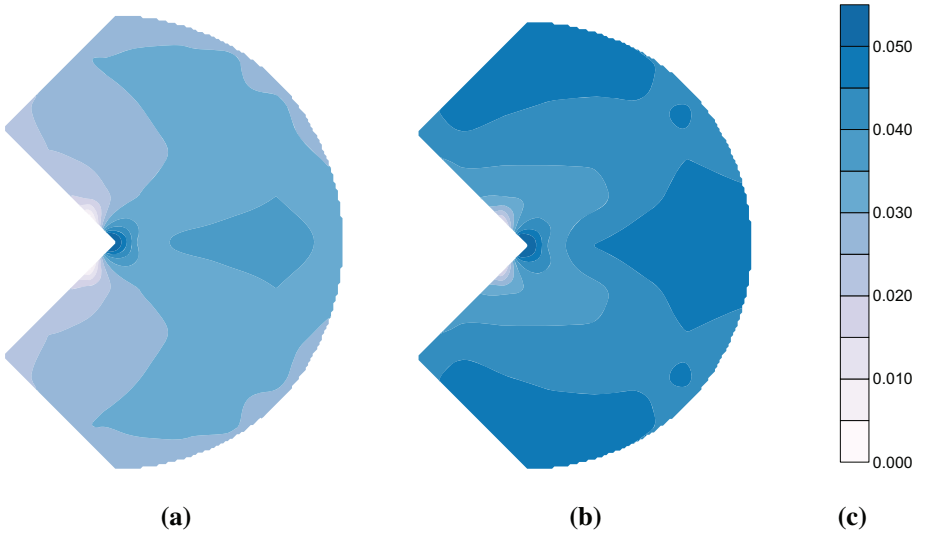

Figure 17. Displacement error in the internal points. (a) ImprIGABEM. (b) IGABEM. (c) Legend.

is plotted over the internal domain with reference to the ImprIGABEM results, Figure 17(a), and to the IGABEM results, Figure 17(b). The more intense blue underlines a higher error for the IGABEM results.

The maximum error values are 3 and 7%, respectively, i.e. the IGABEM approach provides an error that is more than double. The percentage of the domain with an error less than 3% is more than 90% for the proposed approach whereas it is 25% for the classical approach.

5. Conclusions

An improved IGABEM approach was presented. In the usual IGABEM approach, the boundary conditions are directly applied to the control variables regardless

on the position of the control points. As these points are not always interpolatory in the governing field variables, a numerical error may be introduced. The improved proposed procedure was demonstrated to be clear of such an error. It requires the inversion of matrices C whose computation is very fast due to their banded property. Some numerical examples were presented to demonstrate that the present approach is able to overcome the drawback and to provide higher accuracy.

Disclosure statement

No potential conflict of interest was reported by the authors.

ORCID

Vincenzo Mallardo http://orcid.org/0000-0002-1915-3758
Eugenio Ruocco http://orcid.org/0000-0003-2433-6230

References

Beer, G., Marussig, B., & Duenser, C. (2013). Isogeometric boundary element method for the simulation of underground excavations. *Géotechnique Letters, 3*, 108–111.

Costantini, P., Manni, C., Pelosi, F., & Sampoli, M. L. (2010). Quasi-interpolation in isogeometric analysis based on generalized B-splines. *Computer Aided Geometric Design, 27*, 656–668.

De Luycker, E., Benson, D. J., Belytschko, T., Bazilevs, Y., & Hsu, M. C. (2011). X-FEM in isogeometric analysis for linear fracture mechanics. *International Journal for Numerical Methods in Engineering, 87*, 541–565.

Embar, A., Dolbow, J., & Harari, I. (2010). Imposing Dirichlet boundary conditions with Nitsche's method and splinebased finite elements. *International Journal for Numerical Methods in Engineering, 83*, 877–898.

Hughes, T. J. R., Cottrell, J. A., & Bazilevs, Y. (2005). Isogeometric analysis: CAD, finite elements, NURBS, exact geometry and mesh refinement. *Computer Methods in Applied Mechanics and Engineering, 194*, 4135–4195.

Mallardo, V., & Ruocco, E. (2014). An improved isogeometric boundary element method approach in two dimensional elastostatics. *CMES: Computer Modeling in Engineering and Sciences, 102*, 373–391.

Munoz, J. J. (2008). Modelling unilateral frictionless contact using the null-space method and cubic B-spline interpolation. *Computer Methods in Applied Mechanics and Engineering, 197*, 979–993.

Peake, M. J., Trevelyan, J., & Coates, G. (2013). Isogeometric boundary element analysis using unstructured T-splines. *Computer Methods in Applied Mechanics and Engineering, 254*, 197–221.

Piegl, L., & Tiller, W. (1997). *The nurbs book*. Berlin: Springer.

Sevilla, R., Fernández-Méndez, S., & Huerta, A. (2008). NURBS-enhanced finite element method (NEFEM). *International Journal for Numerical Methods in Engineering, 76*, 56–83.

Sevilla, R., Fernández-Méndez, S., & Huerta, A. (2011). 3D NURBS-enhanced finite element method (NEFEM). *International Journal for Numerical Methods in Engineering, 88*, 103–125.

Simpson, R. N., Bordas, S. P. A., Lian, H., & Trevelyan, J. (2013). An isogeometric boundary element method for elastostatic analysis: 2D implementation aspects. *Computers and Structures, 118*, 2–12.

Simpson, R. N., Bordas, S. P. A., Trevelyan, J., & Rabczuk, T. (2012). A two-dimensional isogeometric boundary element method for elastostatic analysis. *Computer Methods in Applied Mechanics and Engineering, 209-212*, 87–100.

Szabo, B., & Babuska, I. (1991). *Finite element analysis*. New Jersey, NJ: John Wiley & Sons.

Verhoosel, C. V., Scott, M. A., de Borst, R., & Hughes, T. J. R. (2011). An isogeometric approach to cohesive zone modeling. *International Journal for Numerical Methods in Engineering, 87*, 336–360.

Wang, D., & Xuan, J. (2010). An improved NURBS-based isogeometric analysis with enhanced treatment of essential boundary conditions. *Computer Methods in Applied Mechanics and Engineering, 199*, 2425–2436.

Wrobel, L. C., & Aliabadi, M. H. (1996). *The boundary element method, Vol. 2: Applications in solids and structures*. New Jersey, NJ: John Wiley & Sons.